Astron. Astrophys. 323, 250–258 (1997)

ASTRONOMY
AND
ASTROPHYSICS

The dispersion of radio waves in the solar corona

Arnold O. Benz and Paolo Pianezzi

Institute of Astronomy, ETH-Zentrum, CH-8092 Zürich, Switzerland (benz @astro.phys.ethz.ch)

Received 6 November 1996 / Accepted 16 December 1996

Abstract. Different arrival times of the two magnetoionic modes in solar radio bursts have been detected. The bursts are from four decimetric radio events showing narrowband millisecond spikes. They have been observed with 2 ms and 0.5 ms time resolution, respectively, by the Ikarus and Phoenix spectrometers of ETH Zurich. The four events have been selected because of their low polarization. The arrival times of the left and right circularly polarized modes have been compared by cross-correlation. In all cases the weaker mode is delayed by a fraction of a millisecond. Several tests have been carried out to ensure the significance of the delay.

The delay is interpreted by the difference in group velocity of the two modes due to dispersion in the coronal plasma. Simple models show that the observed difference in travel time is consistent with this interpretation. It suggests that the radiation is polarized in the *ordinary mode* at the location where the polarization originates. If the polarization originates in the original source region, the possible emission processes are limited to the ones radiating in ordinary mode. More likely, the polarization seems to originate at higher altitude e.g. in a quasi-transverse region. In both cases the delay is proportional to the longitudinal component of the magnetic field in the medium of propagation.

Key words: radiative transfer – Sun: corona – Sun: flares – Sun: radio radiation

1. Introduction

Magnetoionic theory predicts two modes of propagating electromagnetic radiation, the ordinary and extraordinary mode. The ordinary mode has the larger group velocity. Hence a sharply peaked unpolarized signal propagating through a plasma will arrive in ordinary mode first, and the extraordinary mode will be delayed. The detection of a delay would open exciting possibilities for coronal investigations: (i) The sense of polarization of the delayed mode uniquely defines the predominant direction of the longitudinal magnetic field in the medium of propagation. (ii) The delay is proportional to the longitudinal component of magnetic field. (iii) If the polarization originates in the source and is imbedded in the dispersing medium, the delay and the observed polarization define the predominant mode of emission. The dominant mode is an important characteristic of the emission mechanism. Thus, its determination can discriminate between different processes.

The two modes may not originate in the source of emission. One mode only may be emitted and be partially transformed into the other during propagation. In the following the source of emission is distinguished from the spatial origin of the polarization, e.g. the site of depolarization, from where the two modes propagate independently.

Delays between the two circular modes can originate in various ways. Some metric type III bursts start with high circular polarization and show a declining degree of polarization toward the end of the burst (Gopala Rao 1965; Slottje 1974; Santin 1976). This amounts to a delay between the peaks of the left and right circular modes of up to one second. It is much bigger than propagation in the corona could produce and is interpreted as an effect of the different cutoff frequencies of the two modes. For a given frequency the ordinary mode can escape from closer to the plasma frequency. Fast particles arrive first at a given height and excite fast Langmuir waves having frequencies close to the plasma frequency. Therefore the ordinary mode is excited first and is more intense (Benz et al. 1979).

Another previously reported case of delays between modes are fine structures of decimetric type IV bursts. Chernov & Zlobec (1995) find no consistent trend in the sign of the delays and interpret them by multipath effects and quasi-transverse regions. Furthermore they consider the delays as too large for dispersion effects by the corona. Wentzel et al. (1986) failed to detect a delay between modes in metric type I bursts with an upper limit of 4 ms.

Here we report on delays in the arrival times of the two circular modes in narrowband spikes observed in the decimeter range. Narrowband spikes of solar radio emission have been known for more than three decades (cf. Benz 1986 for a review). They have been discovered in the various frequency bands as soon as the necessary time resolution became available and form a separate type of emission distinguishable in the spectrum from other short emissions (e.g. Isliker & Benz 1994). Their typical duration decreases from 100 ms at 300 MHz to less than 10 ms

Send offprint requests to: A. O. Benz

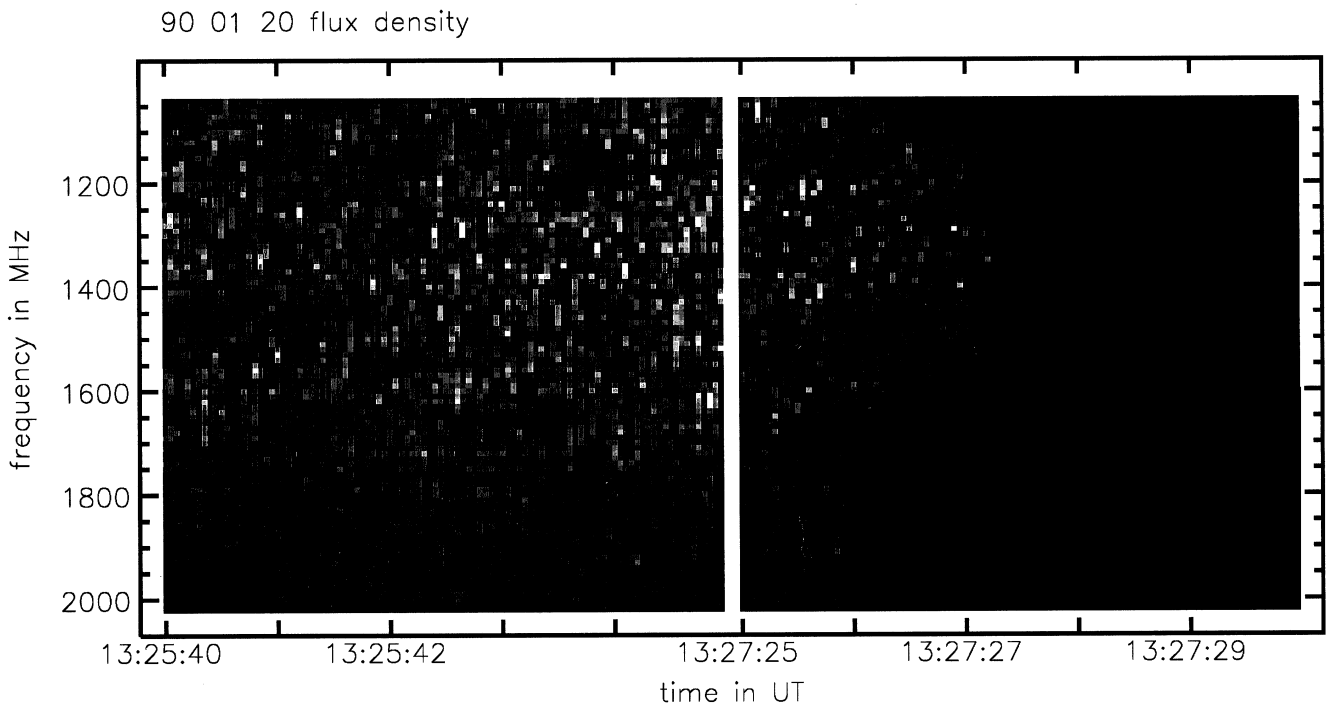

Fig. 1. Broadband observation of a narrowband spike event on 1990 January 20 observed by the Phoenix spectrometer of ETH Zurich. A gliding background of 1 s scale was subtracted. Single spikes show as bright, vertical dashes. During the gap the instrument measured 4 frequencies with high time resolution (cf. Fig. 2, top)

at 3 GHz (Güdel & Benz 1990). Spikes are the shortest solar radio emissions and thus the ideal signal to search for group velocity delays.

Spike bursts from the center of the solar disk tend to be highly polarized. The average polarization significantly decreases toward the limb (Güdel & Zlobec 1991). At low frequencies, Benz & Güdel (1987) have noticed a definite relation between the sense of observed spike polarization and the polarity of the leading spot of the associated active region. Assuming that the polarity of the emission region is the same as the leading spot, they find that the spikes are emitted in the ordinary mode. Güdel & Zlobec (1991) distinguish between metric spikes, occurring mostly below 300 MHz in association with type III bursts, and decimetric(or microwave) spikes above 300 MHz in association with hard X-rays. For the decimetric type and the same assumptions they find extraordinary emission mode. From their findings one may conclude that metric and decimetric spikes are different modes of emission or suffer different propagation conditions.

The total bandwidth of spikes is extremely small. Typical values range from 0.2–3% (Csillaghy & Benz 1993). Estimates of the source size based on bandwidth and VLBI observations (Benz et al. 1996) suggest values of the order of 100 km. This leads to brightness temperatures of the spike radiation up to 10^{15} K, being strong evidence for a coherent emission process. Csillaghy & Benz (1993) find no difference in the frequency dependence of duration and bandwidth in metric and decimetric spikes. This may be taken to indicate that both kinds of spikes are produced by the same mechanism.

Several emission mechanisms for spikes have been proposed, but none is generally accepted. The electron maser has been suggested by many authors (e.g. Holman et al. 1980; Melrose & Dulk 1982; Aschwanden 1990; Robinson 1991; Kuncic & Robinson 1992). It only operates at a very low ratio of thermal to magnetic energy density, β, and predicts extraordinary mode except for a restricted range of β. Upper hybrid, z-mode and Bernstein-mode instabilities have been proposed by Zhelznyakov & Zaitsev (1975), Vlahos et al. (1983), Tajima et al. (1990), Güdel & Wentzel (1993), and Willes & Robinson (1996). These waves require wave–wave coupling to be converted into propagating radio emission, which then is predominantly in ordinary mode.

High time resolution observations of decimetric narrowband spikes are presented in the following section. In Sect. 3 the method is described how the delay has been measured for the first time and how its accuracy was estimated. The results are compared with theoretical expectations and discussed in view of the physics of spike emission and propagation in Sect. 4.

2. Observations

High time resolution data of narrowband spikes have been recorded with two spectrometers of ETH Zurich. The *Ikarus* spectrometer (Perrenoud 1982) operated during the 21st solar cycle from 100–1000 MHz. This instrument was rebuilt into the

Table 1. Overview on the parameters of the spike observations.

date	start time [UT]	time resolution [ms]	frequencies [GHz]	number of spikes
1982/06/04	13:38:14	2	0.361, 0.362, 0.363, 0.364	120
1990/01/20	13:24:00	0.5	1.1, 1.4, 1.7, 2.0	35
1990/02/15	11:36:35	0.5	1.1	21
1990/02/16	10:58:20	0.5	1.1	49

Phoenix spectrometer with a frequency range 0.1–3 GHz operating during the 22nd solar cycle (Benz et al. 1991). Both instruments observed the full Sun with a 7m parabolic disk and a linear, log-periodic feed. The circularly polarized modes are found before pre-amplification by phase-shifting the linear modes in a hybrid. Both spectrometers were frequency-agile, integrating one channel at a time with a resolution of 0.5 ms. A total of 2000 flux densities and circular polarization values can thus be measured per second. The observing frequencies and bandwidths are selectable and controlled by the system computer. One scan in frequency can contain from 1 to 500 observing channels, yielding time resolutions from 0.5 ms to 250 ms.

The receiver is calibrated daily against a reference noise source to find the relation between the digital readings at the A/D converter and antenna temperature. Also, the zero levels of left and right circular polarization are determined. The antenna up to the first switch is calibrated with the quiet Sun several times per year, using single-frequency observations from other observatories. This provides a relation between antenna temperature and physical flux units, as well as the zero point of circular polarization.

In 1982/83 and 1992 special programs have been carried out to measure with high time resolution. The Sun was monitored in a wide band to automatically register solar bursts. If a burst is detected at a given frequency, the system computer switches to a reduced list of channels near that frequency and records for a given time. Then it goes back to the broadband list to record an overview and to test whether the burst continues. This sequence is repeated until the enhanced emission vanishes. We have used the broadband data to identify spike events and to select events with intermediate and low polarization. An example of a broadband recording from 1.03 to 2.02 GHz is shown in Fig. 1. The resolution in this figure is 50 ms in time and 10 MHz in the spectrum. The spikes are marginally resolved in frequency, but not in time, in agreement with the average values found in previous work. Fig. 1 is interrupted at 13:25:45 for 90 seconds of high time resolution single frequency recording at 1.1, 1.4, 1.7 and 2.0 GHz in 250 ms intervals each.

Examples of spike recordings with high time resolution in a single channel are shown in Fig. 2. The digitization steps are clearly visible. In the top of Fig. 2 a weakly polarized spike is shown. The left circular polarization is slightly delayed. An example of a more polarized spike is shown in the bottom of Fig. 2. The weak right polarization mode makes it much more difficult to measure the delay.

Table 1 lists the observing parameters of the four selected events. In the event of 1982/06/04, observed by the Ikarus spectrometer, the instrument swept through the four channels every 2 ms. The observing frequencies are in the low-frequency part of an event that extended up to 1 GHz.

Only well developed, isolated bursts, well recorded over their entire lifetime, were used for the statistical analysis. Their number is given in Table 1. They were added into one time serie for each event and then cross-correlated.

3. Data analysis

3.1. Choosing the method

To extract the delay between modes turned out to be a challenging task in statistics. Noise and digitization steps produce considerable effects. Several methods have been developed and tested with an artificial time profile, $F_{R,L}(t)$, sampled from a gaussian form, to which noise, $N_{R,L}$, observed at a time of no bursts has been added:

$$F_{R,L}(t) = A_{R,L} \exp\left[(t - \tau_{R,L})^2/\tau_w^2\right] + N_{R,L}(t) \quad . \tag{1}$$

$A_{R,L}$ and τ_w are amplitudes and width, respectively, as approximately observed on 90/02/16 (Fig. 2, bottom). R and L are indices for the two modes. The delay $\tau = \tau_R - \tau_L$ is a free input parameter to be reproduced by the method extracting it from noisy profiles. Eq. (1) assumes that the noise does not depend on the strength of the signal. This is not the case in reality. However, the bursts were generally weaker than the background and the error is small. Artificial profiles as defined in Eq. (1) were used to test the statistical methods and their effects on the result as a function of the delay and the noise level.

All methods to eliminate the noise have failed. In a first attempt, the data was Fourier transformed, suppressed at the frequencies where only noise contributes, and transformed back. The discrete structure of the data makes this method ineffective since the power spectrum of the noise also contains considerable contributions at lower frequencies. The Fourier method did not improve the accuracy of the delay measurement in the test data. In a second attempt the data was fitted with a smooth curve. However, all fitting routines used just spread the noise over a longer interval. Thus the measured delay and its error remained practically unchanged.

The delay of single spikes has been measured by three methods: (i) the cross-correlation between the two modes, (ii) the

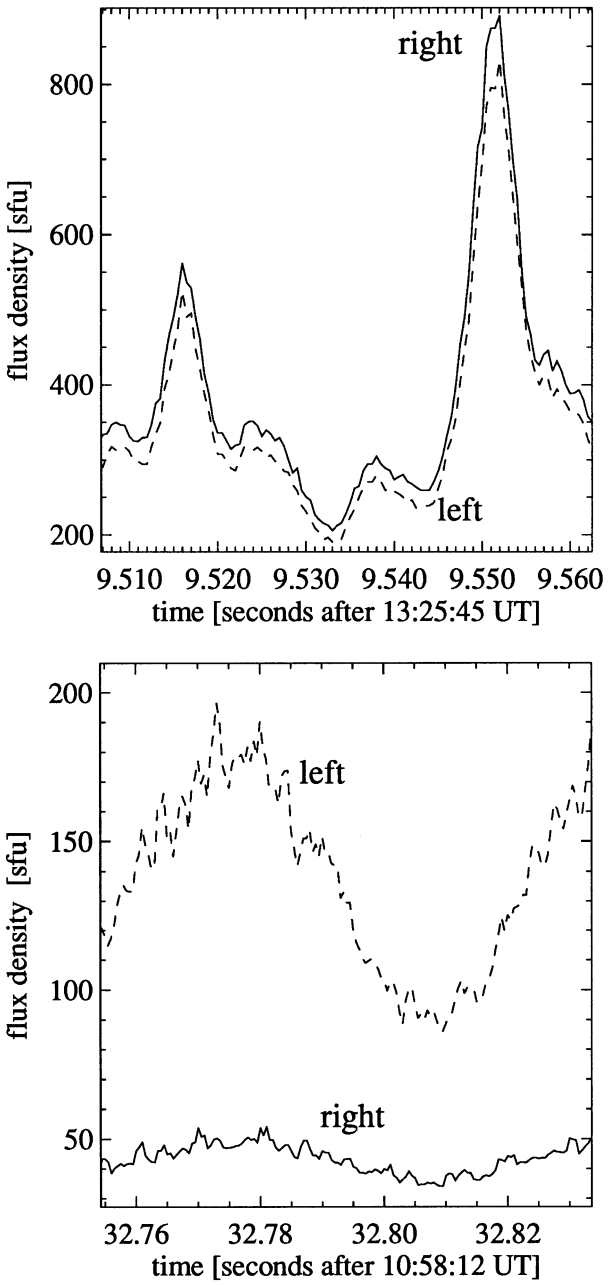

Fig. 2. Single-frequency recordings of single narrowband spike bursts by the Phoenix spectrometer of ETH Zurich. The time resolution is 0.5 ms. The left circular polarization mode is shown with a full curve, right circular polarization is dashed. *Top:* spikes on 1990 January 20 (cf. Fig. 1) at 1.4 GHz, *Bottom:* a spike on 1990 February 16 at 1.1 GHz.

'center-of-mass' time of each mode defined by

$$\tau_{cm}^{R,L} = \frac{\sum_{i=1}^{n} t_i \, F_{R,L}(t_i)}{\sum_{i=1}^{n} F_{R,L}(t_i)} \quad , \tag{2}$$

where the flux density $F_{R,L}(t_i)$ is observed during the interval with the mean time t_i, and (iii) the median method, i.e. the time at which the area under the time profile splits into equal parts.

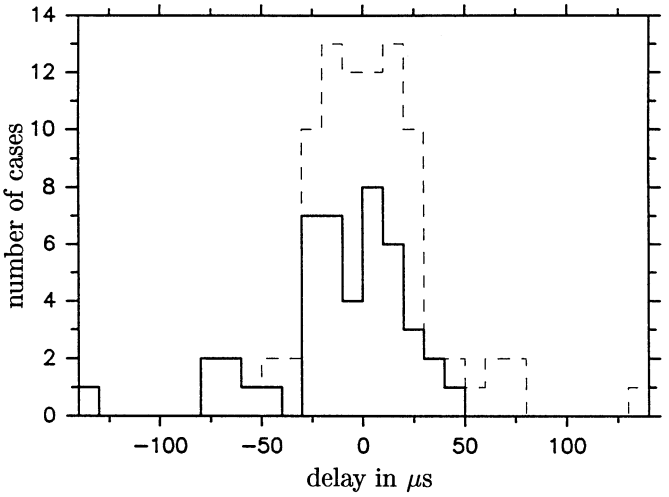

Fig. 3. The delay of 45 model spikes was measured in artificial, noisy model spikes (cf. Eq. 1) having an input delay of $\tau = 0$. The full histogram shows the number of cases per 25 μs bin. The dashed histogram is the distribution neglecting the sign of the delay.

All three methods are severely limited by the noise. The center-of-mass method and the median method are able to reliably detect delays of one tenth of the original time resolution. The center-of-mass method weights the wing of an event more than the center. The cross-correlation method is slightly less sensitive, but depends less on the shape of the burst than the other two methods. When applied to real data, the scatter of the delays in single spikes was smallest for the cross-correlation.

The time delay between left and right polarization of 45 artificial, single bursts with different noise has been measured by cross-correlation and is displayed in Fig. 3. The time delay, τ, in the model (cf. Eq. 1) has been put to zero. The scatter of the measured delays is the result of the noise. The distribution has a standard deviation of 28.2 μs. The mean value of the measured delay is -8.4 μs with a mean error of $\pm$4.2 μs. This test proves that the cross-correlation method can determine the delay with an accuracy of a fraction of the original resolution (in this case 500 μs).

Even better results were achieved when a whole sequence of spikes was cross-correlated together. The sensitivity of this method to detect small delays in artificial data was clearly superior to the other methods. In particular, the deviation from the input delay was significantly lower than averaging the delays of single spikes extracted by any of the three methods.

3.2. The cross-correlation function

The cross-correlation coefficient is defined by

$$C(l) = \frac{\sum_{i=1}^{n-l} F_L(t_i) F_R(t_{i+l})}{\left(\sum_{i=1}^{n} F_L(t_i)^2 \times \sum_{i=1}^{n} F_R(t_i)^2\right)^{1/2}} \, . \tag{3}$$

The summation in the numerator is over all pairs possible for the lag l; n is the total number of measurements in the time profile.

F_L and F_R are the observed values, assumed to be superpositions of the intrinsic spike emissions, L and R, and noise, ΔF_L and ΔF_R, respectively:

$$F_L(t_i) = L(t_i) + \Delta F_L(t_i) \ , \tag{4}$$

$$F_R(t_i) = R(t_i) + \Delta F_R(t_i) \ . \tag{5}$$

Let the standard deviations of the noise be σ_L and σ_R. They are assumed to be unrelated in the following derivations. Tests have shown that the covariance of the noise in the left and right modes is zero except at zero lag. This is a known instrumental effect and will later be accounted for. Neglecting non-zero covariance and using the gaussian law of error propagation, the standard deviation of the cross-correlation is

$$\sigma_C^2(l) = \sum_{i=1}^{n-l} \left(\frac{\partial C(l)}{\partial L(t_i)} \right)^2 \sigma_L^2 + \sum_{i=1}^{n-l} \left(\frac{\partial C(l)}{\partial R(t_{i+l})} \right)^2 \sigma_R^2 \ . \tag{6}$$

Since the time delay is determined from the central points of the cross-correlation function and the background has been subtracted, the following approximation for small lags can be used:

$$\sum_{i=1}^{n-l} L(t_i)^2 \approx \sum_{i=1}^{n} L(t_i)^2 \ , \tag{7}$$

$$\sum_{i=1}^{n-l} R(t_{i+l})^2 \approx \sum_{i=1}^{n} R(t_i)^2 \ . \tag{8}$$

Assuming $\sigma_L \approx \sigma_R = \sigma$, consistent with the observed background data and the weakness of the spikes, Eq. (6) can be put into the form

$$\sigma_C(l) = \frac{\sigma}{\sqrt{n}} \sqrt{\frac{n(1-C(l))}{\sum_{i=1}^{n} L(t_i)^2} + \frac{n(1-C(l))}{\sum_{i=1}^{n} R(t_i)^2}} \ . \tag{9}$$

The accuracy of the cross-correlation increases linearly with the flux density of the spikes and with the square root of the number of data points, n. Eq. (9) demonstrates how the signal-to-noise ratio is improved by cross-correlating a long sequence of data.

3.3. Measuring the time delay

If the noise is small enough, the resolution of the delay measurement from cross-correlations can be considerably better than the original time step of the data. For this improvement the cross-correlation function is interpolated by a polynomial of third order. A spline interpolation was used taking into account the known standard deviation σ_C. The interpolated function therefore does not exactly follow the values of the cross-correlation function, but allows for a mean deviation of σ_C.

The time delay τ between the modes is the lag of the maximum value of the interpolated correlation function C_i. The time delay is defined by the zero point of the derivative, $C_i' = 0$. The error in the measurement of τ is calculated from the Taylor expansion of the function C_i' (e. g. Chatfield 1989),

$$C_i'(l) = C_i'(l_0) + C_i''(l_0)(l - l_0) + ... \tag{10}$$

With l_0 sufficiently close to τ, the derivative can be approximated to the first degree in $(l - l_0)$. At $l = \tau$ the first derivative vanishes, and from from Eq. (10) follows

$$\tau \approx l_0 - \frac{C_i'(l_0)}{C_i''(l_0)} \ . \tag{11}$$

Gaussian error propagation in Eq. (11) yields for the standard deviation in τ

$$\sigma_\tau^2 = \sigma_{l_0}^2 + \left(\frac{1}{C_i''(l_0)} \right)^2 \sigma_{C_i'}^2 + \left(\frac{C_i'(l_0)}{C_i''(l_0)^2} \right)^2 \sigma_{C_i''}^2 \ . \tag{12}$$

Since l_0 is a chosen point of reference, $\sigma_{l_0} = 0$. C_i' near τ is of the order of 10^{-5} and can therefore be neglected. Thus only the second term in Eq. (12) is relevant, and

$$\sigma_\tau \approx \frac{\sigma_{C_i'}}{C_i''(l_0)} \ . \tag{13}$$

The derivative can be approximated by

$$C_i'(l) \approx \frac{C_i(l) - C_i(l + \Delta l)}{\Delta l} \ , \tag{14}$$

where Δl is the time resolution of the interpolated cross-correlation function C_i. Thus

$$\sigma_{C_i'} = \frac{\sqrt{2}}{\Delta l} \sigma_{C_i} \ , \tag{15}$$

Inserting Eq. (15) into Eq. (13) and putting $C_i' \approx C'$, the standard deviation of the delay measurement finally becomes

$$\sigma_\tau \approx \frac{\sqrt{2}\, \sigma_C}{C_i''(l_0) \Delta l} \ . \tag{16}$$

The value of $C_i''(l_0)$ has been calculated from test data and found to be constant over a large interval around τ.

3.4. Other sources of error

The error given in Eq. (16) is only the statistical influence of noise. Two more sources of error must be considered.

Most serious are instrumental effects introduced by the spectrometer. Fortunately, data of two instruments could be used with completely different high-frequency equipment (cf. Sect. 2). As a test of the instruments, the background noise in the two modes was cross-correlated. Fig. 4 (left) shows an example of the results. There is a prominent peak at zero lag, indicating that the noise in right and left circular polarization is not entirely independent. The reason is that the feed is linearly polarized.

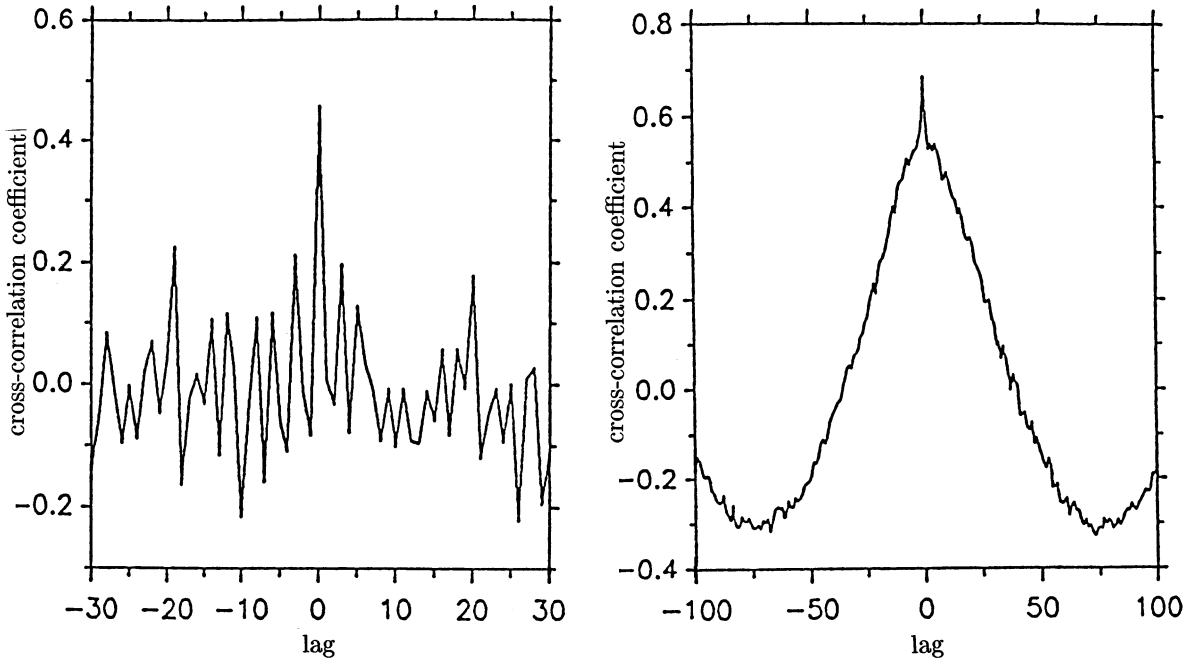

Fig. 4. The cross-correlation coefficient vs. time lag in units of 500μs, *Left:* from background data on 90/02/15, *Right:* from a single spike on 90/02/15.

Table 2. Measurements of the time delay between modes. A positive sign indicates a delay of the left circular mode of polarization relative to the right mode. The coordinates of the associated Hα flares are taken from Solar-Geophysical Data Comprehensive Reports. The second line of 1990/02/16 (b) includes only the 9 strongest spikes.

date	delay [μs]	polarization	solar coord. assoc. Hα
1982/06/04	89 ± 1	R 30%	S10/E55
1990/01/20	56.1 ± 0.5	R 5%	S26/E50
1990/02/15	-208 ± 160	L 65%	N34/W06
1990/02/16 a	-251 ± 55	L 65%	N21/W40
1990/02/16 b	-130 ± 34		

The two linear polarizations are converted into right and left circular polarizations by $\pm 90^\circ$ phase changes in a hybrid. All the noise added to the linearly polarized signal before the hybrid is therefore correlated in circular polarization. The effect has only been detected in the 1990 data and is possibly due to one of the additional switches in the signal path of the Phoenix spectrometer. Fig. 4 (right) shows the effect on the data. It enhances the correlation at zero lag, but is completely absent at lag $+\Delta t$ and $-\Delta t$, where Δt is the original time resolution. The effect was found to be variable in time. The only way to avoid it, was to delete the correlation of zero lag in the interpolation.

The second systematic effect we have encountered originates if the background level changes with time. A trend in the background moves the peak time into the direction of the higher background. If the trends in the right and left mode are the same, the effect on the time delay between modes cancels. If not, a fictitious delay is introduced. To avoid the effect, the background in the interval was carefully examined before cross-correlation and, if necessary, a minimum envelope was subtracted. Times of high spike rate have been omitted, so that the background could be determined reliably. It is reasonable to assume that the remaining effect cancels in the average over a large enough sample.

3.5. Investigation and results

Table 2 contains the relevant results for the four observations. First, the details of the investigation are summarized for each event.

82/06/04: The four recorded frequencies are close enough to be integrated into one channel. This effectively reduces the time resolution to 2 ms. A 27s time interval has been selected and a minimum envelope subtracted to avoid the effect of background fluctuations.

90/01/20: The event has a high rate of spikes. A total of 35 single frequency recordings of 250 ms each have been selected, which contained one full spike each. The background was subtracted individually in each interval. Out of the 35 spikes, 16 were at 1.1 GHz, 9 at 1.4 GHz, and 5 for both 1.7 and 2.0 GHz with an average total duration of 24, 20, 14, and 17 ms, respectively. The 35 intervals were merged into one time series and cross-correlated together.

90/02/15: Same as in the 90/01/20 event. A total of 21 spikes, all at 1.1 GHz, were cross-correlated. Their average duration was 56 ms.

90/02/16: Same as in the 90/01/20 event. A total 49 intervals were merged. The average spike duration at 1.1 GHz was 64 ms. For a second cross-correlation, only the 9 strongest spikes were selected and analyzed separately (average duration 69 ms). The selection increased the accuracy, but the resulting delay between modes was statistically not different from the larger sample.

The method described in Sect. 3.4 yields an average of the delays weighted by the spike flux. The measured delays (Table 2) are statistically significant except for 1990/02/15. Note that the delays cannot be readily compared to the test data in Fig. 3, where a particular model for the spike emission (equal amplitude) has been used.

The error given in Table 2 has been determined from Eq. (16). It is the *statistical* error of the average value caused by the noise. We expect that the accuracy is reduced considerably by systematic errors in the first two events and that the *effective* error is more than the value given in Table 2. In the last two events the polarization is high and the noise of the weaker mode is more influential.

The scatter in the intrinsic delay of individual spikes cannot be measured accurately. Nevertheless, there is no indication from the analysis of single spikes that the delays of an event have different signs. In all four cases the weaker mode of circular polarization is delayed. Assuming that the longitudinal component of the magnetic field at the origin of the polarization and in the decisive part of propagation has the same sign, the spikes have been emitted in $ordinary\ mode$.

3.6. Polarization

Furthermore, the average degree of polarization can be readily determined from the cross-correlation function at zero lag,

$$C(0) = \frac{\sum_{i=1}^{n} F_L(t_i) F_R(t_i)}{\left(\sum_{i=1}^{n} F_L(t_i)^2 \times \sum_{i=1}^{n} F_R(t_i)^2\right)^{1/2}} \ . \tag{17}$$

The polarization is expressed as

$$P = \frac{1-a}{1+a} \ , \tag{18}$$

where a is the average ratio of left to right circular polarization, $a =< F_R > / < F_L >$. If the noise is sufficiently small, Eq. (17) becomes

$$C(0) \approx \frac{2a}{(1+a^2)} \ . \tag{19}$$

Thus,

$$a \approx \frac{1-\sqrt{1-C(0)^2}}{C(0)} \ . \tag{20}$$

Inserting Eq. (20) into Eq. (18), the degree of circular polarization then is given.

Since the noise is correlated at zero lag, the cross-correlation function, $C(0)$, is interpolated from the adjacent values at $l = \pm\Delta t$ and $l = \pm 2\Delta t$. The statistical noise on the result is extremely small and is negligible compared to the systematic calibration errors. Thus the degree of polarization given in Table 2 is rounded off to five percent accuracy.

It is interesting to compare the sense of the observed circular polarization with the hemisphere where the associated Hα flare was seen. In 1990 (sunspot cycle 22) the two left circularly polarized events occurred in the Northern hemisphere and the marginally right circularly polarized event originated from a flare in the Southern hemisphere. The right polarized event of 1982 – in the previous cycle, when the global polarity of the Sun was opposite – occurred in the Southern hemisphere.

The magnetic polarity of the leading spot of the active region was determined from magnetograms published in Solar and Geophysical Data. It was found to be consistent with the general trend for positive polarity in the Northern hemisphere during cycle 21, and negative polarity during cycle 22. Assuming that the magnetic polarity of the emitting region is given by the leading spot and no polarization reversals occur during propagation, the observed polarization would indicate that the decimetric spikes of the 1982/06/04 event originated as predominantly ordinary mode, the other three events (one of them marginal) as extraordinary mode.

The trend for extraordinary mode as determined by the leading spot hypothesis is consistent with the findings of Güdel & Zlobec (1991). However, it contradicts the observed delays, when interpreted as a dispersion effect.

4. Discussion

Can the observed time delay between modes be the effect of different group velocities of the propagating radiation? Relative delays of the two modes result in a magnetized plasma, where the indices of refraction differ for the two modes. If the wave frequency ω is well above the cutoff and $|\cos\theta|/\sin^2\theta \ll \Omega_e/2\omega$ (where θ is the propagation angle relative to the magnetic field, and Ω_e is the electron gyrofrequency), the quasi-longitudinal approximation of the index of refraction is valid. Thus

$$n_{o,x} \approx \left(1 - \frac{X}{1 \pm Y}\right)^{1/2} \ , \tag{21}$$

where $X = \omega_p^2/\omega^2$ (ω_p being the plasma frequency) and $Y = \Omega_e\,|\cos\theta|/\omega$. The upper and lower sign in Eq. (21) correspond to the ordinary and extraordinary mode, respectively. The approximation (21) holds in most of the corona since generally $\omega \ll \omega_p \ll \Omega_e$, except near sources of plasma emission and regions of nearby perpendicular propagation (e.g. Benz 1993). Since $n = ck/\omega$, the group velocity $v_{o,x} = \partial\omega/\partial k$ can be derived from Eq. (21). The time delay τ between modes is the integral along the ray path from the source to the observer

$$\tau = \int \left(\frac{1}{v_x} - \frac{1}{v_o}\right) \mathrm{d}s \ . \tag{22}$$

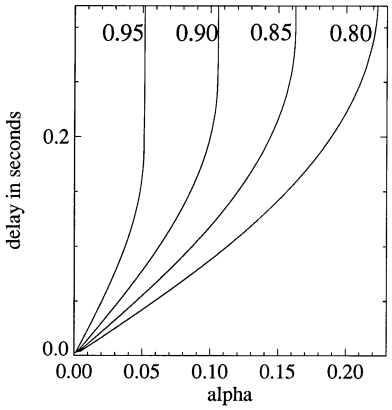

Fig. 5. Time delay between circular modes as a function of $\alpha = \Omega_e|\cos\theta|/\omega_p$ for various starting values X_0 indicated in the figure ($X_0 = \omega_{p0}^2/\omega^2$). A density scale height of $H_n/\cos\Phi = 10^{10}$ cm has been assumed.

We have evaluated Eq. (22) for a simple model, assuming a constant ratio α, where

$$\alpha = \frac{\Omega_e|\cos\theta|}{\omega_p} = \frac{Y}{\sqrt{X}} \quad . \tag{23}$$

Assuming a constant angle θ, a constant α implies both constant Alfvén velocity and constant β in the plasma where the difference in the integral of Eq. (22) is significant. The constant ratio also implies the same scale height for the magnetic field and the square root of the electron density. Therefore the delay can be easily evaluated as a function of α and X_0, the starting value of X at the site where the polarization originates. A barometric density model, $n(h) = n_0\exp(-h/H_n)$, is assumed. Hence Eq. (22) can be transformed to

$$\tau \approx \frac{H_n}{\cos\Phi}\int_{X_0}^{0}\Big(\frac{1}{v_x(X,\alpha)} - \frac{1}{v_o(X,\alpha)}\Big)\frac{\mathrm{d}X}{X} \quad . \tag{24}$$

Φ is the angle between the vertical and the ray path. The result is shown in Fig. 5 for a density scale height corresponding to a temperature of $2\cdot10^6$ K. At the cutoff frequency of the extraordinary mode, the delay becomes infinity since the group velocity of the extraordinary wave vanishes. A decreasing X_0 lets the polarization originate at a higher frequency relative to the local plasma frequency, reducing the delay.

Comparing Fig. 5 with the results of Table 2 immediately demonstrates that the observed delays are many orders of magnitude smaller than may be expected from spike sources. Either the spike polarization originates at extremely small values of X_0 and α (requiring small Y_0) or small density scale heights or both. For $X_0 \ll 1$ and $Y_0 \ll 1$, Eqs. (21) and (22) can be approximated to lowest order in X and Y, yielding

$$\tau \approx \frac{4H_n}{3c\cos\Phi}X_0Y_0 \quad . \tag{25}$$

It corresponds to the lower left corner of Fig. 5 and small X_0. Fig. 5 and Eq. (25) indicate the dependence of the delay on the coronal model: At large τ it is dominated by X_0, and at small τ by H_n and Y_0 in addition.

Model A

Model A assumes that the polarization originates in the spike source. Lower limits on X_0 and Y_0 can be derived from proposed emission mechanisms. For illustration we use the model of Willes & Robinson (1996). Based on observations of harmonic spikes they propose as typical source parameters $X_0 \gtrsim 0.0625$ and $Y_0 \gtrsim 0.0833$. Thus an observed delay of 100 μs can only be explained if the scale length, $H_n/\cos\Phi \lesssim 4.3\cdot10^8$ cm. This dimension is consistent w typical diameters of coronal loops as seen in soft X-rays (e.g. Golub etal. 1990). However, to avoid a large delay outside the dense structure, the density must decrease by more than 6 of these small scale lengths, i.e. the density in the source must be higher by more than a factor of e^6 than in the ambient medium. Although observations may not exclude this,model A is not supported by observations. We may note that model A does not allow for maser emission requiring X_0 and Y_0 close to unity or larger.

Model B

As an alternative to extremely small density scale lengths it is conceivable that the spike emission originates as highly polarized radiation, but is transformed into a mixture of modes in the higher corona, where the local plasma frequency and electron gyrofrequency are much lower than the observing frequency, ω. The values of X_0 and Y_0 can then be considerably lower than in the source. Two such processes have been proposed: (i) The crossing of a quasi-transverse region and (ii) scattering on lower-hybrid waves.

(i) In an inhomogeneous medium of propagation with a quasi-transverse magnetic field, the two modes are coupled. If the coupling is intermediate, i.e.

$$Q := \Big(\frac{\omega}{\omega_t}\Big)^4(1-\omega_p^2/\omega^2)^{5/2} \approx 1 \quad , \tag{26}$$

where

$$\omega_t := \Big(\frac{\alpha^3\omega_p^5 H_B}{4c}\Big)^{1/4} \quad , \tag{27}$$

an incoming circularly polarized wave becomes fully linearly polarized and subsequently gets completely depolarized by Faraday rotation. For $\omega^2 \gg \omega_p^2$ in the quasi-transverse region and $\omega \approx \omega_t$, it follows from Eq. (27) that

$$X_0Y_0 \approx \Big(\frac{4c}{\omega_p H_B}\Big)^{3/4}\alpha^{-5/4} \quad . \tag{28}$$

Using a conventional upper limit on the magnetic scale height of $H_B < 10^{10}$ cm, Eq. (25) yields $\tau > 0.3\alpha^{-5/4}\mu$s. Thus the depolarization in a quasi-transverse region is compatible with the observed delays for $\alpha = \Omega_e/\omega_p > 1.5\cdot10^{-2}$.

(ii) The deflection of radio waves on lower-hybrid waves has been proposed by Wentzel et al.(1986) for the production of two modes (equivalent to depolarization) in type I bursts. It may be

noted here that the depolarizing lower-hybrid waves would have to occur on similar heights in the corona for spikes and type I bursts (Wentzel 1997). The conservation conditions require

$$\omega_r + \omega_{lh} = \omega_d \quad , \quad \mathbf{k_r} + \mathbf{k_{lh}} = \mathbf{k_d} \quad . \tag{29}$$

The deflection changes the degree of polarization depending on the angle of incidence between the radio wave and the lower-hybrid wave. Since the frequency of the lower-hybrid wave is small compared to the radio wave, the frequency remains practically unchanged for the deflected wave. The deflection can take place at much lower X_0 and Y_0 than in the source of emission. Thus the delay between modes can be as small as observed, if the combination of deflected and direct waves does not introduce additional delays.

Both processes for reduced polarization in spikes have starting values X_0 and Y_0 at higher altitude and lower ω_p and Ω_e than in the source. Using a conventional density scale height of $H_n/\cos\Phi = 10^{10}$cm and an observed $\tau \approx 10^{-4}$s, Eq. (25) yields $X_0 Y_0 \approx 2 \cdot 10^{-4}$. They are consistent with the emission model quoted above if the polarization originates at a site where e.g. the density and magnetic field are both reduced by more than an order of magnitude compared to the source.

5. Conclusions

A method to measure the delay between the arrival time of the two magnetoionic modes has been developed and tested. It has been successfully applied to weakly polarized narrowband spikes of solar flares at decimeter wavelengths. The measured delays are of the order of 100 μs.

In all four events the weaker mode was found to be delayed. The weakly polarized spikes thus appear to be predominantly ordinary mode at the origin of the polarization. One magnetoionic mode can couple to the other mode in a quasi-transverse region or be partially deflected into the other mode by low-frequency turbulence. Thus the source of emission may not coincide with the common starting point of the two observed modes.

The observed delays beteen 50 and 250 μs are extremely short. The difference in group velocities of the two modes is a possible cause of delays, but it causes considerably longer delays if the modes originate near the plasma frequency (assuming $\omega_p \approx 10\Omega_e$) and typical coronal conditions are used. If the origin of polarization is in the source of emission, the proposed emission mechanisms require scale lengths $H_n \lesssim 3 \cdot 10^7$cm. Alternatively, the radiation could be emitted fully polarized and be transformed to less polarization in a quasi-transverse region or by lower-hybrid waves. The delay would then be produced only during propagation from this site to Earth. The second scenario is consistent with spike emission models producing fully polarized radiation.

Ordinary mode emission is naturally predicted by spike theories based on plasma waves as the primary waves. They are preferentially transformed into ordinary mode radio waves. The observations thus support this if the mode is not changed in a quasi-transverse region (weak mode coupling, $Q \lesssim 1$). Alternatively, emission in extraordinary mode is possible if the coupling is strong. It would then agree with the leading spot rule. Although this rule is not well understood, it adds some credibility to the hypothesis of the extraordinary mode of emission.

Since there is no qualitative difference in metric and decimetric spike bursts, it has been proposed that they are produced by the same process (Csillaghy & Benz 1993). If metric and decimetric spikes have the same emission mechanism, the observations may be best interpreted by ordinary mode emission as in metric type III bursts, partial transformation into the other mode and a more complex field geometry in the decimetric sources inverting the leading spot rule in the majority of the cases. The confirmation of this scenario needs additional information on the flare geometry based on spatially resolved observations.

Acknowledgements. It is a pleasure to thank Dr. H. Isliker for his help in the evaluation of the statistical accuracy of the results. We also acknowledge helpful discussions with M.J. Aschwanden, M. Güdel, and D.G. Wentzel. The operation of the Zürich radio spectrometers is a team effort. We would like to thank in particular W. Stehling for his help in running the instruments. Their construction and some of the data analysis are financed by the Swiss National Science Foundation grant 20-46656.96

References

Aschwanden M.J., 1990, A&AS 85, 1141
Benz A.O., 1986, Solar Phys. 104, 99
Benz A.O., 1993, Plasma Astrophysics, Kluwer, Dordrecht
Benz A.O., Güdel M., 1987, Solar Phys. 111, 175
Benz A.O., Güdel M., Isliker H., Miszkowicz S., Stehling W., 1991, Solar Phys. 133, 385
Benz A.O., Graham D., Isliker H. et al., 1996, A&A 305, 970
Benz A.O., Urbarz H.W., Zlobec P., 1979, A&A 79, 216
Chatfield C., 1989, in: The Analysis of Time Serie, 4th edition, Chapman & Hall, London
Chernov G.P., Zlobec P., 1995, Solar Phys. 160, 79
Csillaghy A., Benz A.O., 1993, A&A, 274, 487
Gopala Rao U.V., 1965, Australian J. Phys. 18, 283
Golub L. et al., 1990, Nature 344, 842
Güdel M., Wentzel D.G., 1993, ApJ 415, 750
Güdel M., Benz A.O., 1990, A&A 231, 202
Güdel M., Zlobec P., 1991, A&A 245, 299
Holman G.D., Eichler D., Kundu M.R. 1980, in M.R. Kundu & T.E. Gergeley (eds.): Radio Physics of the Sun, IAU Symp. 86, 457
Isliker H., Benz A.O., 1994, A&AS 104, 145
Kuncic Z., Robinson P.A., 1992, Solar Phys. 145, 317
Melrose D.B., Dulk G.A., 1982, ApJ 259, 844
Perrenoud M., 1982, Solar Phys. 81, l97
Robinson P.A., 1991, Solar Phys. 134, 299
Santin P., 1976, A&A 49, 193
Slottje C., 1974, A&A 32, 107
Tajima T., Benz A.O., Thaker M., Leboeuf J.N., 1990, ApJ 353, 666
Vlahos L., Sharma R.R., Papadopoulos K., 1983, ApJ 275, 374
Wentzel D.G., 1993, ApJ 407, 380
Wentzel D.G., 1997, Solar Phys., in press
Wentzel D.G., Zlobec P., Messerotti M., 1986, A&A 159, 40
Willes A., Robinson P.A., 1996, ApJ 467, 465
Zhelznyakov V.V., Zaitsev V.V., 1975, A&A 39, 107